Biosensors and Bioelectronics 198 (2022) 113820

Contents lists available at ScienceDirect

Biosensors and Bioelectronics

journal homepage: www.elsevier.com/locate/bios

Dual-mode sensing of biomarkers based on nano 3D Cu-Flo. @AuNPs-electrocatalyzed oxidation of glucose inducing in-situ H_2O_2-generation system

Jianping Guo [a], Shijie Li [a], Junying Wang [b,*], Junping Wang [a,**]

[a] State Key Laboratory of Food Nutrition and Safety, Tianjin University of Science & Technology, 29 the Thirteenth Road, Tianjin Economy and Technology Development Area, Tianjin, 300457, PR China
[b] The Biotechnology Research Institute (BRI) of Chinese Academy of Agricultural Sciences (CAAS), PR China

ARTICLE INFO

Keywords:
Cu-Flo. nanosheet
H_2O_2-generation
Electrocatalysis
ECL-Biosensing

ABSTRACT

A bimodal 3D-electrochemiluminescence (ECL) analysis method was developed, which integrated simpleness, label-free, high-throughput and real time detection together. Firstly, a novel 3D copper-based nanosheet micromaterial (Cu-Flo. NMs) coupled with gold nanoparticles/Cysteine (Cu-Flo.@AuNPs-Cys) was prepared to use as the versatile label for both colorimetric and ECL techniques. The 3D-Cu-Flo.@AuNPs-Cys having glucose oxidase-like activity could catalyze glucose to produce H_2O_2 in situ, which was further found to be capable of exhibiting a 30.95-fold higher ECL-intensity for luminol than bare glassy carbon electrodes (GCE). Taking advantages of the 3D-Cu-Flo.@AuNPs-Cys above, a colorimetric and ECL-channel sensor (GCE/3D-Cu-Flo.@AuNPs-Cys) were constructed simultaneously for glucose detection. The fabricated sensor displayed a wide linear range (Glucose: 0.001–50 mmol L^{-1}, AFP: 2.25 × 10^{-7}–225 ng mL^{-1}), impressive low limit of detection (Glucose: 1.27 × 10^{-7} mol L^{-1}, AFP: 1.92 × 10^{-8} ng mL^{-1}, S/N = 3) and acceptable recovery (Glucose: 94% ~ 104%, AFP: 96.04% ~ 102.29%) in practical sample. Furthermore, the biosensor showed ultrafast (0.5 min) analysis efficiency, high stability for 6 cyclic potential scans and satisfactory reproducibility for 7 repeated tests. These results demonstrated the proposed 3D dual-modal ECL-biosensor for biomarkers detection had a great potential in clinical diagnostics, promoting the application in biomedical researching and POCT.

1. Introduction

Electrochemiluminescence (ECL), a signal-emission process in a redox reaction of electrogenerated reactants, is favored by many scholars due to the high accuracy, rapidity, sensitivity and portability in emergency cases(Hu et al., 2019; Praoboon et al., 2021). Recently, ECL have been widely applied to the fields of medicinal analysis, food safety and biomarker assay(Jie et al., 2018; Liu et al., 2021). Among various electrochemiluminescence (ECL) systems, the collocation of luminol-H_2O_2 is well-studied and commonly used in bioassays owing to its sensitive luminescence, low excitation potential, high luminescent efficiency and inexpensiveness(Wang et al., 2019a). However, the traditional ECL reaction of luminol occurs in solution phase, resulting in scattered luminescence region, massive energy loss(Khoshfetrat et al., 2019). It is well-known that reactive oxygen species (ROSs) derived from hydrogen peroxide (H_2O_2) effectively boost the ECL intensity of luminol, hence H_2O_2 is often used as a coreactant(Xue et al., 2019). However, the ECL-signal stability is often affected due to the subtleness of H_2O_2 by external conditions (pH, concentration, temperature, etc.) (Cheng et al., 2020). These are the defects that need to be solved for luminol-H_2O_2 system.

In order to overcome ECL-instability caused by direct addition of H_2O_2, some ECL processes were driven by the production of H_2O_2 in situ based the natural enzymatic catalyzed, such as glucose oxidase(Wang et al., 2013), alcohol oxidase (AOx) (Carro et al., 2018), which can improve the ECL stability to some extent. However, the application of the natural enzyme is easily limited by external factors, such as intrinsic instability, too narrow pH operational condition and relatively high cost (Quintero-Jaime et al., 2021). In recent years, electrocatalysis production of H_2O_2 through nanozyme instead of natural enzyme has attracted

* Corresponding author.
** Corresponding author.
E-mail addresses: wangjunying@caas.cn (J. Wang), wangjp@tust.edu.cn (J. Wang).

https://doi.org/10.1016/j.bios.2021.113820
Received 29 June 2021; Received in revised form 5 November 2021; Accepted 17 November 2021
Available online 24 November 2021

increasing interest due to the low durability, resistance of high temperature and extreme pH.

To further enhance sensor's sensitivity, many electroactive materials with catalytic abilities for glucose were employed in the development of enzyme-free biosensors(Olvera and Monaghan, 2021). The highly active surface area of the materials played a critical part in sensing response (Geng et al., 2017; Lee and Lin, 2021). For example, Wang et al., (2019) reported the fabrication of three-dimensional (3D) flower-like nickel (II)-terephthalic acid (Ni(TPA)) metal-organic framework (MOF) doped with the single-walled carbon nanotubes (SWCNT), which exhibited excellent electrocatalytic activity for non-enzymatic glucose sensing. Roushani et al., (2021) fabricated the NiP_2/hollow N-doped carbon nanofiber (NiP_2/CNCNF), which was used directly as a high electrocatalytic and freestanding electrode for non-enzymatic glucose sensing. The research of nano-enzyme sensors based on carbon skeleton was a hot topic due to the high electron transfer-rate and good biocompatibility. Singh et al., (2014) reported a novel nano-enzyme (Pt/f-CNC) coppled carbon nanochips (CNC) with Pt for enzyme-free glucose sensing, further demonstrating the role of carbon materials in effective nano-catalysis and performance.

Cu-based nanoparticles (CuO, Cu_2O, Cu^{2+}), a promising active material (Biniuri et al., 2018; Ma et al., 2019; Zhu et al., 2019a), was also reported that could efficiently catalyze glucose for glucose detection (Zhu et al., 2020). Zhuang's group(Zhuang et al., 2021) fabricated a ternary copper-metal-organic framework (Cu/Cu_2O) on GCE, and the GCE/Cu_2O/Cu exhibited excellent selectivity for glucose and good catalytic performance in the test process. Much carbon nanomaterials (carbon nanotubes, carbon dots, graphene quantum dots, etc.) (Clancy et al., 2018; Shen et al., 2016) were utilized for enzyme-free glucose detection owing to their low cost and efficient catalytic characteristic. Nonetheless, the synergistic effect in electrocatalysis field was not yet fully applicated especially regarding mixed hybrids of Cu-based nanoparticles with doping carbon nanomaterials.

Electrochemical polymerization (electro-polymerization) is a simple and useful method to prepare conducting polymers on an electrode surface, where cathodic oxidative coupling proceeds to give polymer deposition(Chen et al., 2021). In this context, the electro-polymerization method was successfully deployed for the synthesis of gold nanoparticles (AuNPs) (Li et al., 2019b). Besides, previous works proved that AuNPs coupled L-Cysteine (L-Cys) exhibited strong ECL intensity of luminol through intramolecular reactions (Gobel et al., 2019; Wang et al., 2020). The integrations of electro-polymerization technology and ECL-system were of great significance to boost the performance of sensors.

More, it was reported for tests of biomarkers that immunoassay was combined with fluorescence (Zhou et al., 2022), chemiluminescence assay (Yang et al., 2018), quartz crystal microbalance (QCM) (Yagmuroglu and Diltemiz, 2020), colorimetric and electrochemistry elegant methods (Fan et al., 2020), etc. However, the methods above were usually single-mode signal readout, high cost, long detection time. The colorimetric methods are usually low sensitivity or even the appearance of "false positive" test results. Based on the above-mentioned views, visualization with naked eye combined with other quantitative analysis dual-mode strategies were continually explored as the most promising approaches.

Inspired by this shining point, we developed a dual-mode self-enhanced ECL-sensor (GCE/Cu-Flo.@AuNPs-Cys-luminol) which combined both colorimetry and electrochemiluminescence for supersensitive and accurate detection of glucose and AFP. Firstly, the electrocatalyst 3D Cu-Flo.@AuNPs-Cys nanozyme for glucose was prepared using the low cost reduced graphene oxide (rGO) by electro-polymerization method, which was completed on glassy carbon electrode (GCE). The green nanomaterial Cu-Flo. was synthesized only with graphene and copper sulfate at room-temperature, which well ensured the human safety and environmental friendliness. The reagents above were cheap and easy to get, reducing the cost. The rough structure and the high load-amounts of 3D-nanosheet microflowers (NMs) resulted in stable and strong ECL signal. In addition, in-site H_2O_2-generation ensured the long-lasting ECL emission and polished the poor ECL performance of luminol. Then, the AFP-blocking and glucose-direct nanozyme-Cu-Flo.@AuNPs-Cys catalytic assays were designed. Finally, the target was decorated to realize quantitative detection rely on the changing ECL intensity.

2. Experimental

2.1. Reagents and instruments

All chemicals and related instruments used in the experiments was listed in supporting information.

2.2. Synthesis of 3D-Cu-Flo. nanosheet microflowers (NMs)

Prior to modification, the bare GCE was polished until a mirror-like surface was obtained before use. First, the ultrathin Cu-Flo. nanosheets were prepared according to the reported methods with major modifications(Zou et al., 2017). (Full details can be found in the supplementary material). During preparation, CuNPs was oxidized into Cu^{2+} in 0.1 mol L^{-1} phosphate buffer solution (pH = 4.1) under applied voltage. Cu^{2+} could in turn transfer to the outer layer from the inner layer of graphene of electrode (Ep: 0.1 V, T: 600 s), thereby causing the formation of the nanosheet micro-flowers structure due to the interaction between the inner graphene and the outer graphene.

2.3. Application of nanozyme-Cu-Flo.@AuNPs-Cys to ECL biosensing

Blocking and direct nanozyme-Cu-Flo.@AuNPs-Cys catalytic assays were designed in this study.

The blocking assay was based on the modulation of the communication between the electrode surface nanozyme-Cu-Flo.@AuNPs-Cys-luminol and glucose by impedance effect upon affinity interaction of immobilized biotin-$Anti_{AFP}$ with the target AFP. Such interaction led to the adsorption of AFP on the surface of GCE/Cu-Flo.@AuNPs-Cys/Biotin-$Anti_{AFP}$ and the subsequent variation of the ECL intensities. According to this operating mechanism, the ECL intensity was inversely correlated with the AFP concentration.

The use of Cu-Flo.@AuNPs-Cys allowed to employ the glucose for the development of much simpler, less expensive and environmentally friendly ECL bioassays depending on nano-enzyme as a bio-recognition element. For the direct assay, the catalytic production of H_2O_2 by nanozyme-Cu-Flo.@AuNPs-Cys was utilized to drive the luminol-ECL process. This approach enabled the direct use of nanozyme-Cu-Flo.@AuNPs-Cys produced H_2O_2, which could act as a coreactant for ECL processes without the introduction of exogenous coreactants, making the system neat, green and simple. In this case the increase in the ECL intensity was directly related with the rate of catalytic reaction and concentration of enzymatic substrates (glucose).

2.4. Fabrication of GCE/Cu-Flo.@AuNPs-Cys/luminol

Subsequently, the films of AuNPs were electrodeposited on the surface of the above prepared GCE/Cu-Flo. in 0.1% $HAuCl_4$ solution (−0.2 V, 200 s). Moreover, the L-Cys was easily decorated on the surface of GCE/Cu-Flo.@AuNPs by Au–S affinity. To further immobilize the luminol molecules, glutaraldehyde was used as crosslinking agent through the aldehyde condensation reaction. Cu-Flo.@AuNPs-Cys-modified carbon electrode was immersed in a stirring, 12-mL reaction solution containing 10 mL glutaraldehyde solution (2.5%) and 2 mL luminol solution (0.02 mol L^{-1}, 1 mL) for 3 h in dark. Then, GCE/Cu-Flo.@AuNPs-Cys/luminol was obtained.

2.5. Fabrication of immune ECL-sensor

The ECL immunosensor was fabricated as follows (Scheme 1C): first, the exposed amino-group on GCE/Cu-Flo.@AuNPs-Cys/luminol were activated by 0.4 mol L^{-1} EDC and 0.1 mmol L^{-1} NHS for 2 h at ambient temperature. Then, 15 μL of antibody solution (40 μg mL^{-1}) was dropped onto the surface of GCE/Cu-Flo.@AuNPs-Cys/luminol for 3 h at 4 °C for immobilization. The unbound antibodies were rinsed completely by

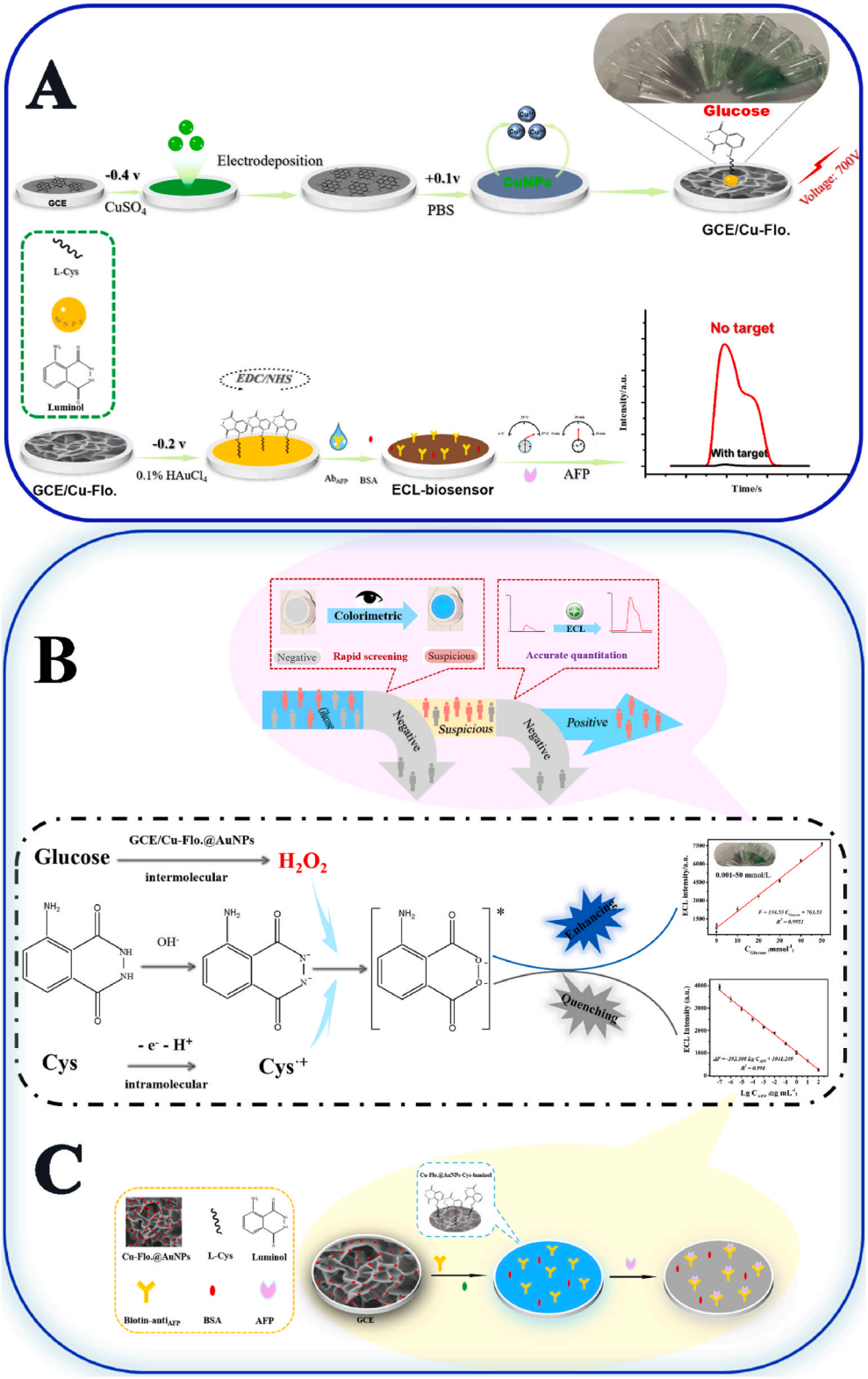

Scheme 1. The conceptual figures of the synthesis process of 3D copper-based nanosheet micro-flowers on electrode and the fabrication process of GCE/Cu-Flo.@AuNPs-Cys-luminol/Ab_{AFP} immune-sensor (A). Mechanism of multiple amplification and schematic illustration of fabrication of (B) 3D GCE/Cu-Flo.@AuNPs-Cys colorimetric and ECL detection for glucose. (C) Construction process of the immune ECL-sensor for AFP.

PBST (0.05%, pH 7.4), following non-specific active sites were blocked by 1% BSA for 30 min at room temperature. Subsequently, GCE/Cu-Flo.@AuNPs-Cys/luminol-Biotin-anti$_{AFP}$ were immersed into AFP-incubation buffer containing different concentrations of AFP for binding the sites of the Anti$_{AFP}$ for 20 min at 37 °C(Xu et al., 2020). The ECL intensity of GCE/Cu-Flo.@AuNPs-Cys/luminol-Biotin-anti$_{AFP}$ and GCE/Cu-Flo.@AuNPs-Cys/luminol-Biotin-anti$_{AFP}$/AFP were tested in glucose-PBS buffer (50 mmol L^{-1}, pH=9.0) solution and then recorded (F_0, F/a.u.), respectively. The ECL bio-sensors fabrication process is shown in Scheme 1A-C.

2.6. Measurement process

In the ECL sensing process, conventional three-electrode system was adopted, consisting of saturated calomel electrode as reference electrode, platinum column as auxiliary electrode. Above resultant electrodes (GCE/Cu-Flo.@AuNPs-Cys/luminol, GCE/Cu-Flo.@AuNPs-Cys/luminol-Biotin-anti$_{AFP}$, 4 mm diameter) were working-electrodes. The 0.2 mol L^{-1} PBS (0.2 mol L^{-1} Na_2HPO_4, 0.2 mol L^{-1} NaH_2PO_4, pH 9.0) containing 0.001–50 mmol L^{-1} glucose was employed as test solution. The ECL measurements were conducted using a commercial ECL system with a scanning range 0–0.8 V and the voltage 700 V. Before the colorimetric analysis, the above GCE/Cu-Flo.@AuNPs-Cys-luminol

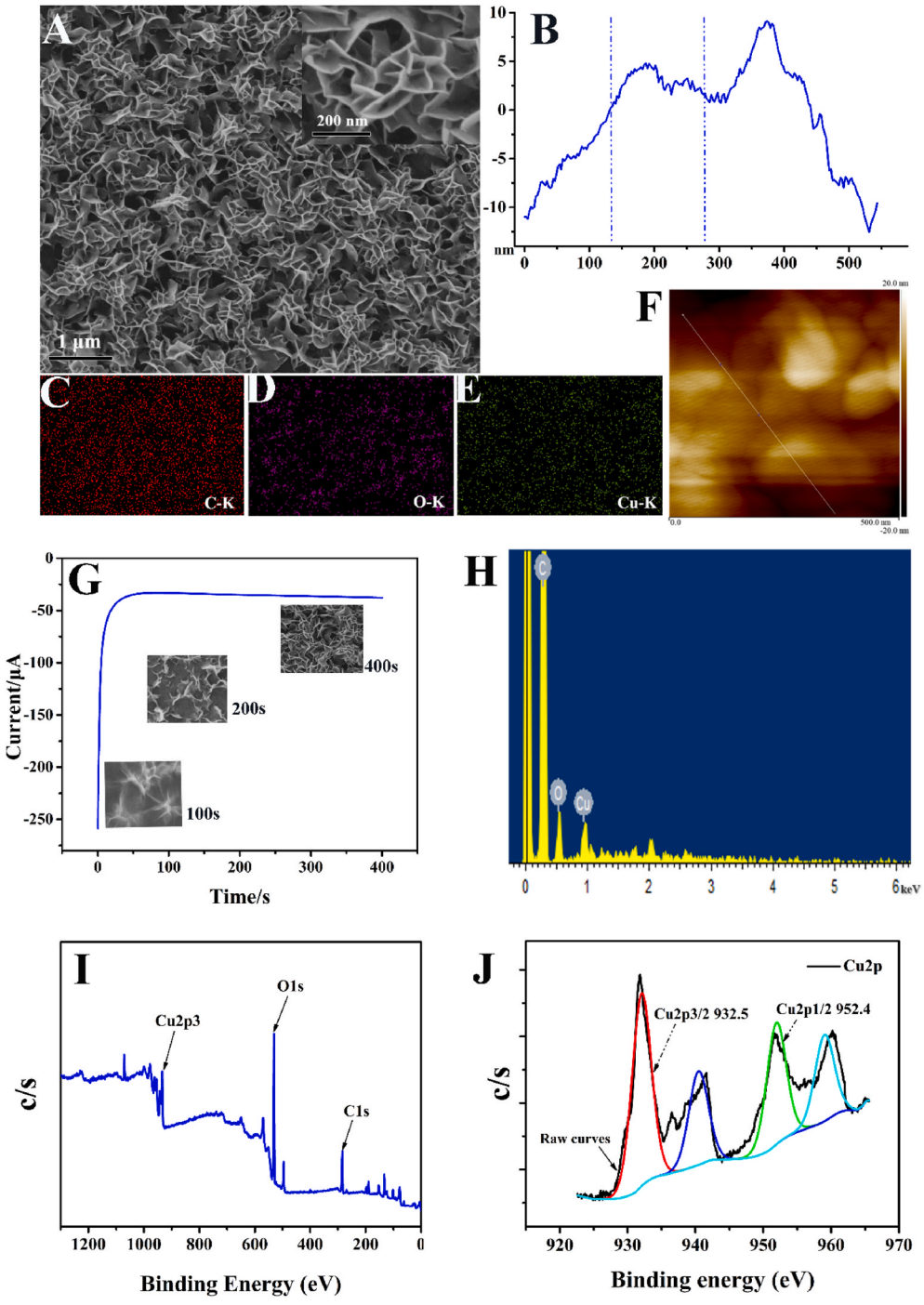

Fig. 1. (A) Overall and partially enlarged SEM images. (B) The line scan profile. (C–E) The elemental mapping analyses. (F) The AFM image. (G) Constant potential deposition curve of CuNPs. (H) EDS image of GCE/Cu-Flo. (I–J) XPS survey spectra of Cu-Flo.

working electrode was firstly immersed in the micro electrolytic-cell for 10 min. And then, 10 μL TMB (0.1 mmol L^{-1}) was added into the miniature electrolytic-cell. The changes of the solution can be recorded by a digital camera after 2 min.

3. Results and discussion

3.1. Characterization of Cu-Flo. NMs and Cu-Flo.@AuNPs

To reveal the morphology and thicknesses of the as-synthesized Cu-Flo. nanosheet micro-flowers (NMs), scanning electron microscopy (SEM) and atomic force microscopy (AFM) were carried out. From the SEM image of Cu-Flo. NMs in Fig. 1A, a flower-like layered assembly structure was clearly displayed. Compared to previous graphene(Zou et al., 2017), wrinkled Cu-Flo. NMs had a larger specific surface area, which implied that it could provide more active sites for subsequent application resulting in better catalytic-activity. Besides, as seen from AFM measurement of the ultrathin Cu-Flo. NMs in Fig. 1F and B, the thicknesses of the Cu-Flo. nanosheets was as thin as ~ 1.4 nm, which facilitated catalytic reactions due to the existence of rich coordinative unsaturated metal sites and carbon-based materials on the surfaces (Wang et al., 2020b). Furthermore, the elemental mappings analyses (Fig. 1C–E) showed that the products contained elements of C, O and Cu, and also verified that these elements were homogeneously distributed in Cu-Flo. NMs. And the morphology for Cu-Flo. NMs were different with the electrodeposition time of CuNPs changing (Fig. 1G). 3D-Cu-Flo. nanosheet micro-flowers acted as a supporting framework could effectively prevent the aggregation of AuNPs, resulting in a smaller average size of gold nanoparticles on GCE/Cu-Flo.@AuNPs. As shown in Fig. S3, AuNPs were uniformly dispersed on the surface of GCE/Cu-Flo. with the particle size of about 15 nm, which was comparable with the result of previous reports(Tan et al., 2017). Due to the connection of Cu-Flo. NMs and AuNPs, the surface of electrode became rugged, which illustrated that AuNPs were successfully modified on surface of Cu-Flo. NMs.

EDS spectra was employed to reveal the presence of different components in 3D-Cu-Flo. NMs. As shown in Fig. 1H, C, O and Cu atoms occupied the element mass. C and O was derived from the rGO. Cu only came from the $CuSO_4$. Hence, the successful preparation of 3D-Cu-Flo. NMs was certified. The XPS analysis of Cu-based GCE/Flo. was also conducted to identify chemical environment. The full survey spectrum

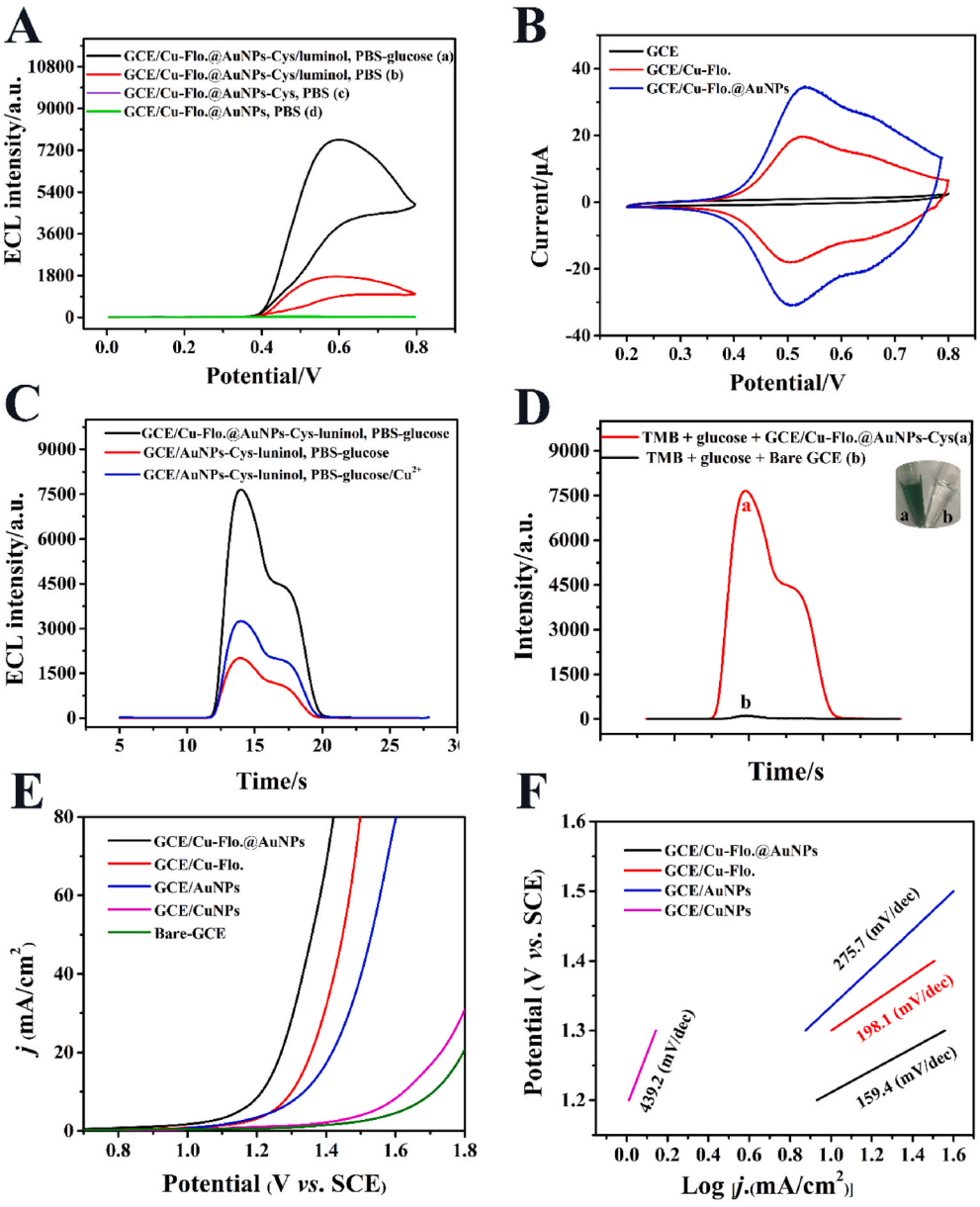

Fig. 2. (A) ECL intensity-potential curves of different modified electrodes: (a) GCE/Cu-Flo.@AuNPs-Cys-luminol (glucose PBS-buffer); (b) GCE/Cu-Flo.@AuNPs-Cys-luminol (PBS-buffer); (c) GCE/Cu-Flo.@AuNPs-Cys (PBS-buffer); (d) GCE/Cu-Flo.@AuNPs (PBS-buffer). (B) CV curves of different electrodes in glucose PBS-buffer. (C) ECL intensity-time curves of GCE/AuNPs-Cys-luminol (Cu^{2+}-solution); GCE/Cu-Flo.@AuNPs-Cys-luminol/GCE/AuNPs-Cys-luminol (glucose PBS-buffer). (D) The ECL intensity of GCE/Cu-Flo.@AuNPs-Cys (a) and bare-GCE (b) in glucose-TMB solution. The inset shows the photograph of the corresponding solution. (E) The polarization curves and Tafel plots (F) of all electrocatalysts for the glucose.

of GCE/Flo., as depicted in Fig. 1I, symptomatized the presence of C, O and Cu element in nanosheet micro-flowers. The XPS spectrum of C and O were derived from the precursor rGO. Fig. 1J displayed the high resolution XPS spectra of Cu2p with the peaks of 932.5 eV and 952.4 eV corresponded to the binding energies of Cu 2p3/2 and Cu 2p1/2, respectively(Bowmaker et al., 2000). The separation of two peaks was 19.9 eV, indicating a +2-oxidation state for the Cu ion(Ma et al., 2019). The reason was that the copper nanoparticles could be oxidated when a constant potential +0.1V was applied to the GCE/Flo. Thus, it proved that the successful synthesis of the 3D micro-flower structure is may attributed to the oxidation of CuNPs under +0.1V constant potential. The reaction equation was as follows:

$$Cu \rightarrow Cu^{2+} + 2e$$

3.2. Electrocatalytic performance of the Cu-Flo.@AuNPs-Cys

To certify the electrocatalysis of Cu-Flo.@AuNPs-Cys, ECL intensity of different modified electrodes were compared. As shown in Fig. 2A, there was no signal because no luminophores existed on electrode (curve c and d). After immobilizing luminol on electrode (curve b), weak signal was monitored due to lack of core-actants, only the excitation of electricity to luminol. Then, ECL emission was greatly improved after adding glucose to electrolyte (curve a), and it also proved that the H_2O_2 was generated after immobilizing on Cu-Flo.@AuNPs-Cys. In addition, it could be seen from Fig. 2A that the initial potential of luminescence was 0.4 V and peak potential was about 0.6 V. Meanwhile, it was found that the peak potential of glucose catalyzed by Cu-Flo.@AuNPs was around 0.5 V (Fig. 2B), which was close to peak potential of ECL. It was inferred that the reason for increase in ECL intensity after addition of glucose was the in-situ generation of H_2O_2, which was produced by electrocatalysis of Cu-Flo.@AuNPs on glucose(Zhu et al., 2020).

As shown in Fig. 2C, the ECL-intensity of Cu-Flo.@AuNPs-Cys-luminol complex exhibited 4-fold higher for glucose catalysis than that of the AuNPs-Cys-luminol. In order to further investigate the catalytic mechanism of the GCE/Flo.@AuNPs-Cys for glucose, the ECL behavior of the AuNPs-Cys-luminol modified electrode was studied in the presence of free Cu^{2+} with same content of that in Flo. (5 mmol L^{-1}) in the electrolyte solution. The electrode showed 1.62-folds enhancement on the ECL intensity, which indicated that the Cu^{2+} facilitated a lot on the catalysis reaction of glucose. The above results confirmed high catalytic effect of the nanosheet micro-flowers Flo. on the Cu-Flo.@AuNPs-Cys-luminol modified electrode. Most importantly, the ultrathin nanosheets and flower-like assembly structure were good platform for supporting AuNPs-Cys-luminol. More, the modification of AuNPs by electro-polymerization(Chen et al., 2021) could effectively prevent the agglomeration of AuNPs-luminol during electrochemical process.

To further confirm the production of H_2O_2, ECL intensity and colorimetric reaction were experimented simultaneously in TMB-glucose PBS-solution. 3, 3′, 5, 5′-tetramethylbenzidine (TMB) was often used to the colorimetric analysis(Zhu et al., 2019a). As shown in Fig. 2D, GCE/Cu-Flo.@AuNPs-Cys catalyzed the oxidation of TMB in the present of glucose and changed the solution from colorless to blue (inset a) with a strong ECL intensity (curve a). In contrast, the color of the solution was not changed (inset b), and the ECL signal was weak on bare-GCE (curve b). These results indicated that Cu-Flo.@AuNPs-Cys had glucose-oxidase-like activity and H_2O_2 was generated indeed. Moreover, Cu-Flo.@AuNPs-Cys was carried out under luminol-system (pH=9.0) and the nano-enzyme activity was little affected by environmental factors. Compared to natural enzymes carried out under an acidic condition generally(Quintero-Jaime et al., 2021), Cu-Flo.@AuNPs-Cys could be applied in a wide range of fields.

Electrocatalytic activities of Cu-Flo.@AuNPs, Cu-Flo., CuNPs and AuNPs catalysts toward the glucose were studied by using linear sweep voltammetry (LSV) with 50 mmol L^{-1} glucose-dissolved 0.2 mol L^{-1} PBS (pH = 9.0) as the electrolyte. As presented in Fig. 2E, Cu-Flo.@AuNPs displayed the best catalytic activity and a lower overpotential of 215 mV (10 mA cm^{-2}), compared with those of Cu-Flo. (301 mV at10 mA cm^{-2}), AuNPs (335 mV at10 mA cm^{-2}) and CuNPs (624 mV at 10 mA cm^{-2}). Furthermore, as shown in Fig. 2F, the Tafel slope of Cu-Flo.@AuNPs (159.4 mV dec^{-1}) was much lower than those of Cu-Flo. (198.1 mV dec^{-1}), AuNPs (275.7 mV dec^{-1}) and CuNPs (439.2 mV dec^{-1}). This was due to the synergic effect of Cu-Flo. NMs and AuNPs membrane(Li et al., 2019b). On the one hand, Cu-Flo. NMs increased the effective surface area and offered a rough surface with petal-like structure. On the other hand, the modification of AuNPs membrane based on Cu-Flo. NMs could expose more catalytic active sites for glucose catalysis. Where the results proved that Cu-Flo.@AuNPs possessed the best electrocatalytic performance for the glucose, which also provided a strategy for subsequent research work.

3.3. Possible mechanism of H_2O_2 formation

The mechanism of the H_2O_2 generation was similar as the enzyme-catalytic mechanism (Quintero-Jaime et al., 2021). Also, previous works have proved that AuNPs exhibited catalytic properties of glucose (Luo, 2010). Moreover, the active sites were the coordination-unsaturated Cu-ions which easily adsorbed the negative charge OH^- from solution. Then, the OH^- could transfer an electron to the electrode forming OH* intermediate and two adsorbed OH* could combine to generate a neutral H_2O_2 molecule with the help of applied electrical field. The H_2O_2 generation mechanism on the surface of GCE/Cu-Flo.@AuNPs could be summarized in the following eqs (1)–(3), (Kang, 2020; Zhu et al., 2020).

$$\text{Glucose} + \text{Cu-Flo.@AuNPs} \rightarrow H_2O_2 \quad (1)$$

and

$$OH^- \rightarrow OH^* + e^- \quad (2)$$

$$2OH^* \rightarrow H_2O_2 \quad (3)$$

3.4. Electrochemical characterization

The construction process and ECL mechanism were explored by ECL, CV, and EIS. The contribution of Cu-Flo.@AuNPs and L-Cys to ECL were also explored. As shown in Fig. 3A, the GCE/Cu-Flo.@AuNPs-Cys-luminol combined with glucose displayed intensive and steady signal. After replacing glucose with H_2O_2, although the initial luminescence intensity was strong, the signal attenuation was distinct. In contrast, the GCE/Cys-luminol showed weak signal, and the signal attenuation was also severe. There were two possible explanations(Bao et al., 2021): On one hand, lack of carrier could not achieve concentrated luminol molecules, and there was no catalyst to generate coreactant. On the other hand, luminol could not be firmly anchored and resulted in leakage of luminol due to lack of carrier. This indicated that the catalytic action of Cu-Flo.@AuNPs could effectively improve the stability.

As a proof-of-concept application, this multi-model ECL-biosensor based on nanozyme Cu-Flo. NMs was firstly fabricated. The corresponding interface properties of stepwise assembly process were monitored by electrochemical impedance spectroscopy (EIS) in 5.0 mmol L^{-1} $K_3[Fe(CN)_6]$ solution containing 0.2 mol L^{-1} KNO_3. As illustrated in Fig. 3B, smaller and smaller semicircles were appeared after Cu-Flo. (curve b) and Cu-Flo.@AuNPs (curve c) were successively decorated onto electrode surface compared with that of bare GCE (curve a), which was owing to the good conductive property of Cu-Flo. NMs and AuNPs (Hu et al., 2019). As expected, the resistances increased obviously when L-Cys and luminol (curve d) were modified onto the above electrode

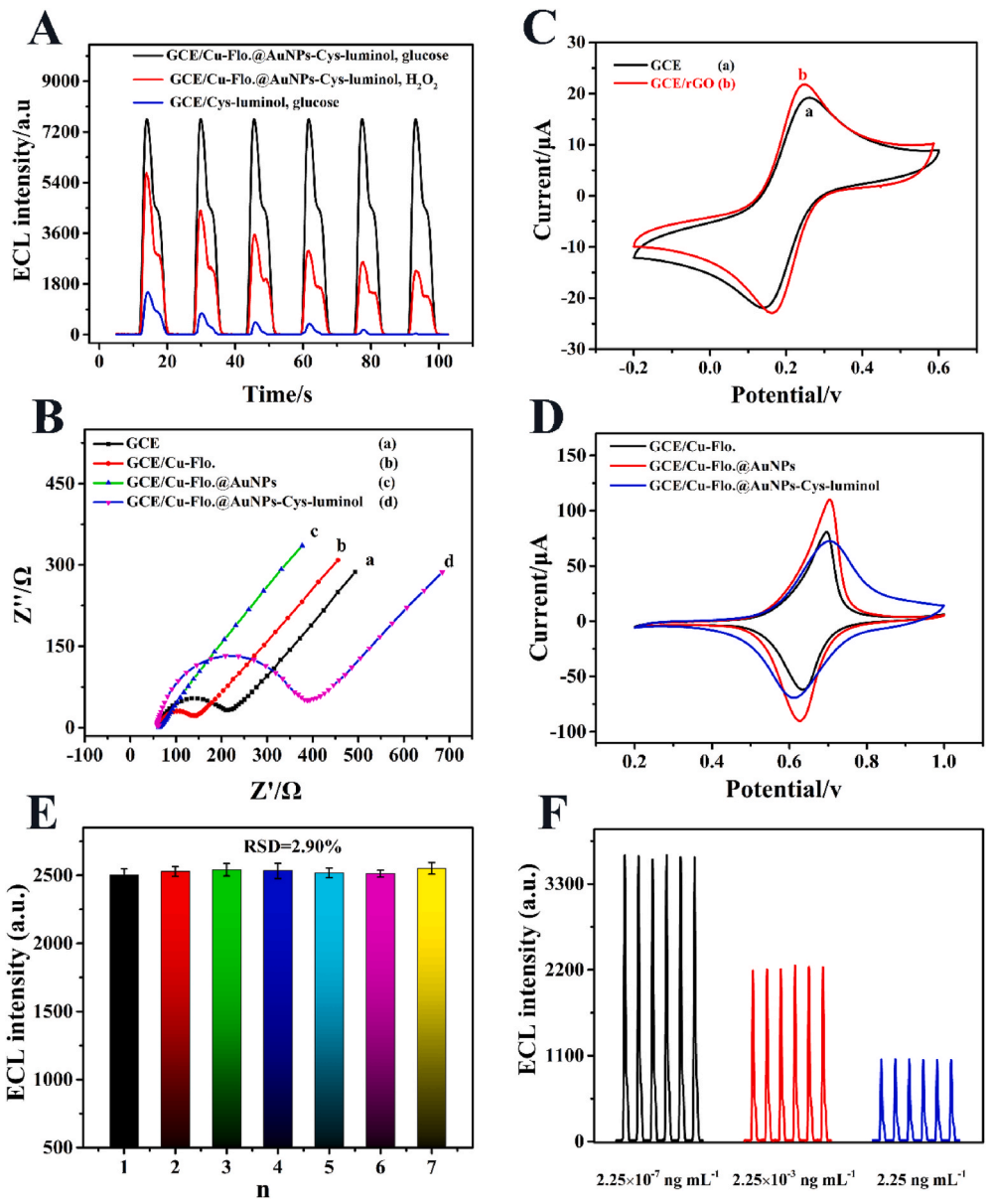

Fig. 3. (A) ECL profiles of different modified electrodes. (B) EIS of GCE, GCE/Flo., GCE/Cu-Flo.@AuNPs and GCE/Cu-Flo.@AuNPs-Cys-luminol in 0.2 mol L^{-1} KNO_3 containing 5 mmol L^{-1} $[Fe(CN)_6]^{3-/4-}$. (C–D) CV curve of GCE (a), GCE/rGO (b), GCE/Cu-Flo., GCE/Cu-Flo.@AuNPs and GCE/Cu-Flo.@AuNPs-Cys-luminol in 1 mmol L^{-1} $K_3[Fe(CN)_6]$ solution. (E) Repeatability tests of a series of 7 electrodes. (F) Continuous cyclic potential scans tests on electrodes.

surface. The reason was mainly attributed to that the low conductivity of L-Cys and luminol, which made electrons transfer between the electroactive probes and the electrode more difficult. Such variations ensured the successful construction of this GCE/Cu-Flo.@AuNPs-Cys-luminol sensor. Fig. 3C and D were the CV curves of modified electrodes in 1 mmol L^{-1} $K_3[Fe(CN)_6]$ solution. It could be seen that redox peak current increased, indicating Cu-Flo. and Cu-Flo.@AuNPs promoted the redox of $[Fe(CN)_6]^{3-}$. When Cys-luminol was modified on electrode, the peak potential spacing increased significantly and current also decreased to a large extent. Consequently, these results firmly proofed that the ECL-sensor was successfully constructed as expected.

3.5. Electrochemical active area

In addition, the effective area (cm^2) of different modified electrodes was calculated respectively based on the results of the cyclic voltammetry test according to the following Randles-Sevcik formula (Wang et al., 2017):

$$I_p = 2.69 \times 10^5 A D^{1/2} n^{3/2} \gamma^{1/2} C$$

Where I_p is the peak current (A); A is the electrochemical effective area (cm^2); D is the diffusion coefficient of molecular ($6.70 \pm 0.02 \times 10^{-6}$ cm^2 s^{-1}); n is the number of electron transfer (1); γ is the scan Rate (0.1 V/s); C is the concentration of electrolyte (1.0 mol cm^{-3}).

The superior performance of the GCE/Cu-Flo.@AuNPs was further illustrated via the electroactive area compared to other modified electrodes. It was assumed that the reaction occurring on the electrode was controlled by the diffusion process. The calculated results were shown in Table S1. The electroactive area of GCE/Cu-Flo.@AuNPs was different-multiple larger than other modified electrodes. The electro-activated area of GCE/Cu-Flo.@AuNPs (1.97×10^{-4} cm^2) was significantly larger than other modified electrodes, which was 5.20 (GCE/rGO), 2.50 (GCE/CuNPs) and 5.92-folds (bare-GCE) enhanced, respectively. Nano Cu-Flo.@AuNPs with higher electroactive area was beneficial to electron-transfer which gave full play to the superiority on assisting

current. Therefore, GCE modified by Cu-Flo.@AuNPs owned the largest electrochemical active area and was applied to the following experiment.

3.6. Analytical performance of ECL-sensor

3.6.1. ECL responses and standard curve

The proposed ECL system was explored for ECL-colorimetric sensing of glucose and ultra-sensitive immunoassay of AFP. The nano-/bio-enzymes ECL system exhibited strong and constant ECL signal in applied voltage condition, showing promising applications in real-time bioassay. Ultra-sensitive and rapid-quantitative monitoring of the blood glucose is becoming significant to the diabetics. Cu-Flo.@AuNPs-Cys could catalyze glucose and produced H_2O_2 quantitatively. As shown in the inset Fig. 4B, the color difference of the reaction system with different concentrations of glucose was very obvious, achieving fast screening, direct readout and rapid identification purpose for samples as negative or positive in point of care (POC). However, the colorimetric-method above is prone to be affected by external interferences (e.g., slight variations of experimental environments, different operating personnel), thus leading to uncertainty, or even the appearance of "false positive" test results. So, the number of suspicious patients has been increased when using the conventional colorimetric analysis than that of the positive patients through the proposed ECL method (scheme 1B). For further precise medical diagnosis, the ECL-test was used for more accurate quantitative analysis. In Fig. 4A, with the increase of glucose concentration, ECL signal increased accordingly.

Under the optimum experimental conditions, the relationship between glucose concentration and the relative ECL intensity (F) was studied. As shown in Fig. 4B, the relative ECL intensity had a good linear relationship with glucose concentration in the range of 0.001–50 mmol L^{-1}. The linear equation was expressed as: $F = 134.53\ C_{glucose} + 763.53$ ($R^2 = 0.9951$), and the limit of detection (LOD) was calculated to be 1.27×10^{-7} mol L^{-1}. Compared with the reported methods, the

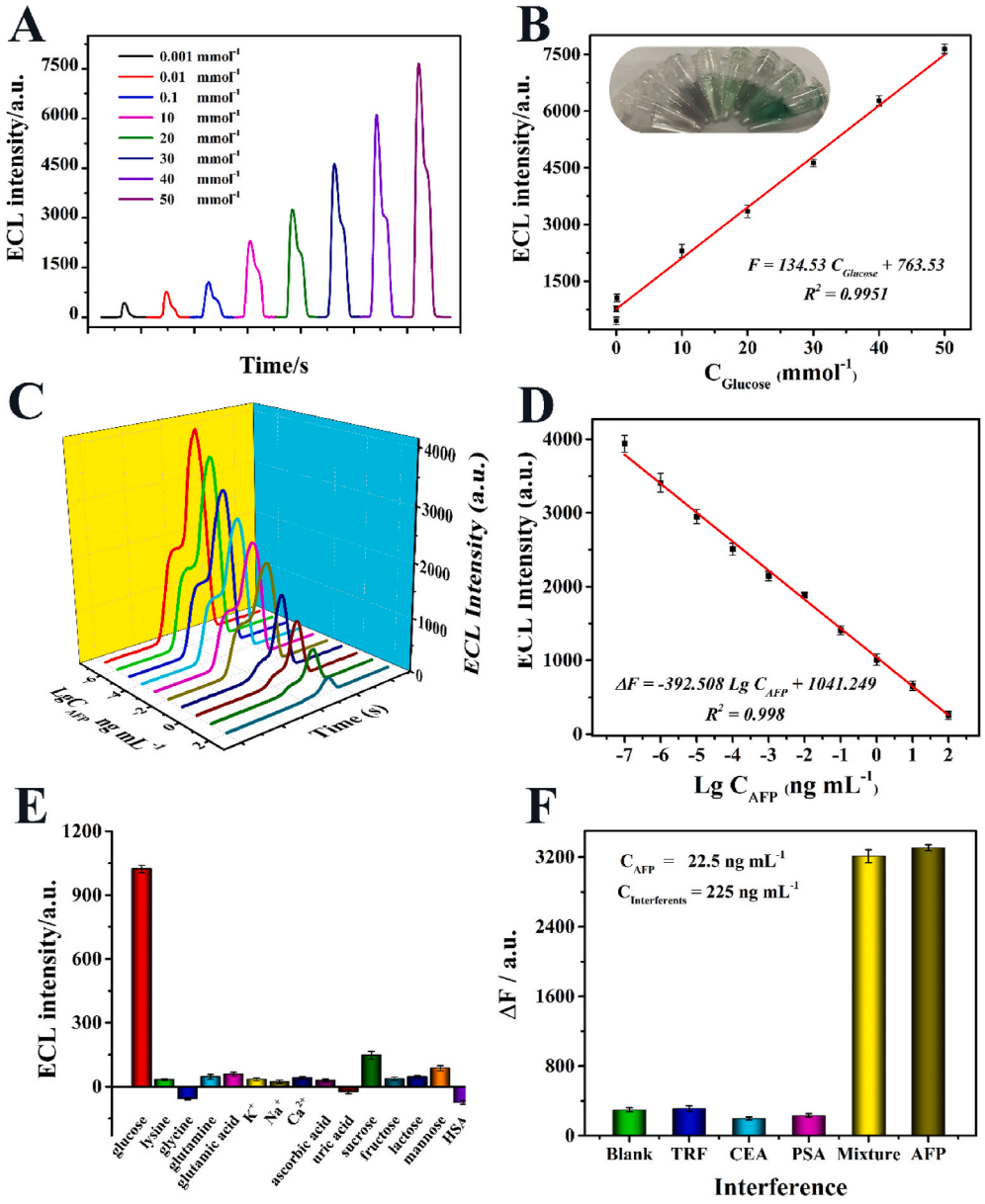

Fig. 4. (A) The linear relationship between glucose concentration and ECL intensity. (B) Linear calibration curves for response to glucose. (C) ECL intensity-time curves of the prepared GCE/Cu-Flo.@AuNPs-Cys-luminol/Biotin-Anti$_{AFP}$ sensor incubated with various concentration of AFP (up to down: 2.25×10^{-7}–225 ng mL^{-1}). (D) Standard curve of immune ECL-sensor (S/N = 3); (E) Interference experiment for glucose determination. (F) Selectivity tests of the fabricated sensor.

analytical performance of this method was also superior and could meet the need of blood glucose determination for diabetic patients (Table 1).

Different concentrations of AFP were also prepared and tested by the proposed blocking ECL-immunosensor under the optimized experimental conditions. As displayed in Fig. 4C and D, with the increase of AFP, more non-conductive Biotin-anti$_{AFP}$-AFP bioconjugate was formed resulting in smaller ECL signal. Owing to the affinity between AFP and GCE/Cu-Flo.@AuNPs-Cys-luminol/Anti$_{AFP}$ also caused the weaker catalytic ability from GCE/Cu-Flo.@AuNPs-Cys, the amounts of ROSs decreased with the increment of AFP. Therefore, the ECL-signal triggered by Cu-Flo.@AuNPs-Cys-luminol was recorded in presence of AFP with different concentrations. As expected, with more AFP, weaker intensity was recorded (Fig. 4C). Additionally, the detailed linearity between the detected signals (ECL intensity) and the logarithm of AFP concentration (C, ng mL^{-1}) were demonstrated in Fig. 4D. Distinctly, the ECL-blocking assay showed the wider linear range (2.25×10^{-7} to 225 ng mL^{-1}) and the lower detection limit (1.92×10^{-8} ng mL^{-1}, S/N = 3). Unquestionably, the results also confirmed the inherent merits including high sensitivity and ultra-low detection limit of ECL technology (Wang et al., 2020a; Zhu et al., 2019c). Comparing with other methods for AFP analysis (Table S2), the integrated-catalysis ECL-sensing platform possessed better accuracy and stability originated from more reliable analytical performance and in-situ H_2O_2-generation.

3.7. Specificity, stability, reproducibility and repeatability of the biosensor

The effects of components in blood and urine that may interfere with glucose determination were tested. Interference experiments were carried out with glucose solution (1.0×10^{-4} mol L^{-1}) (Fig. 4E). The experimental results showed the ECL signals of these substances had no significant difference with the ECL signal of glucose solution. Thus, they did not interfere with glucose determination. In addition, the developed ECL-sensor was also reused by washing the GCE/Cu-Flo.@AuNPs-Cys/luminol with PBS-buffer (pH=7.4). The whole cycle was repeated for 7 runs and the ECL responses dropped substantially after five regeneration cycles (Fig. S9), so an acceptable regeneration cycle should be five (with the RSD 3.34%). The strong signal of GCE/Cu-Flo.@AuNPs-Cys/luminol was due to the stability of Cu-Flo.@AuNPs-Cys nanomaterial on the electrode. The results demonstrated that the developed method had good reproducibility.

Some tumor markers associated with cancer were selected for specificity tests. The selectivity of the immune ECL-sensor towards AFP was studied with CEA, PSA, TRF and mixture with AFP (CEA, PSA, TRF) as interferences, whose concentration was 10-folds of that of AFP. The results were illustrated in Fig. 4F, the ECL-ΔF values of the immunosensor were close to the signal of blank sample for CEA, PSA, TRF. However, when mixture was covered on electrode, ECL intensity was approximately equal to intensity of pure AFP. It indicated that these interfering biomolecules had negligible influence for the highly selective detection of AFP and the sensor had good anti-interference ability. Reusability was a non-negligible property for evaluating the performance of the prepared sensor. Different seven pretreated GCE/Cu-Flo.@AuNPs-Cys-luminol/Biotin-Anti$_{AFP}$ were examined after incubating at 2.25×10^{-4} ng mL^{-1} AFP (Fig. 3E). The RSD of the intra-assay was 2.90%, showing the value of the sensor in repeating utilization. In addition, the stability of the AFP-sensor was investigated by consecutive tests for 6 cycles in three different concentrations (Fig. 3F). It was found that the signals of each concentration were quite steady, indicating the high stability of the established ECL-sensor.

3.8. Real sample analysis

Successful translation of laboratory-based GCE/Cu-Flo.@AuNPs-Cys-luminol ECL-platforms to clinical applications requires multiplex and ultra-trace detection of glucose/AFP from a complex matrix. The glucose in the standard serum samples were determined by this method and enzyme-linked immunosorbent assay (ELISA) method, respectively. The results in Table S3 suggested that the glucose contents determined with the ECL method were in a good agreement with those obtained by ELISA method. The recovery tests had also been performed and the recovery rates showed no significant difference with 100% at the confidence level of 95% based on t-test. The glucose content in the urine samples of two female volunteers had also been determined. As being seen from Table S4, there was no significant difference between the recovery rate and 100% at the confidence level of 95% based on t-test.

To demonstrate whether the proposed AFP-sensor could be used for real sample detection, a series concentration of standard AFP was added into the normal human serum diluted 10-folds with 10 mmol L^{-1} PBS (pH 7.4). The detection results were showed in Table S5 with this method and ELISA, in which the recoveries were in the range of 96.04%–102.29% and 95.94%–101.38%, respectively. By comparison with the ELISA method, the RSDs obtained from the developed method showed acceptable feasibility, indicating the validity of the GCE/Cu-Flo.@AuNPs-Cys-luminol/Biotin-Anti$_{AFP}$ for AFP detection in human serum for clinical diagnosis.

4. Conclusion

In summary, a novel 3D colorimetric and ECL dual-modal biosensor has been constructed for detection of AFP/glucose. Based on the fact that a novel 3D-Cu-Flo.@AuNPs material can catalyze glucose to produce H_2O_2 in situ, which maintained steady ECL signal, a colorimetric and ECL-channel was constructed simultaneously. Integrating the electrical-signal generation and amplification strategies, the enhancing-sensing and blocking-sensing assays were designed for biomarkers detection. As expected, the resulting bioassay exhibited good stability and high

Table 1
Various Previously reported sensors for glucose.

Materials	Methods	Detection range/mol L^{-1}	LOD/mol L^{-1}	Ref.
CuO/NiO–C	Electrochemical	1.0×10^{-7}-4.5×10^{-3}	3.7×10^{-8}	Archana et al. (2019)
ND-Gr-NH	Electrochemical	5.0×10^{-6}-8.0×10^{-5}	1.0×10^{-7}	Huang et al. (2020)
AgNPs@PCN-224	Fluorescence	5.0×10^{-6}-2.0×10^{-3}	8.73×10^{-7}	Du et al. (2020)
AgNC-GOx/Ag^+-FP	Fluorescence	5.0×10^{-5}-5.0×10^{-3}	5.0×10^{-5}	Jiang et al. (2019)
Pt-HMCNs	Colorimetric	1.33×10^{-3}-1.0×10^{-2}	3.54×10^{-5}	Chen et al. (2020)
2D FeS_2@C NSs	Colorimetric	5.0×10^{-7}-5.0×10^{-5}	1.9×10^{-7}	Ding et al. (2020)
Co-MOF	Chemiluminescence	4.0×10^{-8}-8.0×10^{-6}	1.0×10^{-8}	Li et al. (2019a)
Cu-CDs	Chemiluminescence	1.0×10^{-6}-4.8×10^{-7}	3.2×10^{-7}	Duan et al. (2019)
Co-TCPP(Fe)	Chemiluminescence	1.8×10^{-7}-3.1×10^{-5}	5.93×10^{-8}	Zhu et al. (2019b)
C-PANI-TT	Electrochemical	1.0×10^{-6}-1.0×10^{-2}	1.0×10^{-6}	Quintero-Jaime et al. (2021)
C-MEMS	Electrochemical	5.0×10^{-5}-1.0×10^{-3}	4.5×10^{-6}	Jiang et al. (2021)
CNCNF	Electrochemical	4.0×10^{-7}-5.0×10^{-5}	1.3×10^{-7}	Roushani et al. (2021)
MWCNT/ZnO	Photocurrent	1.0×10^{-7}-2.6×10^{-6}	2.08×10^{-7}	Vinoth et al. (2021)
3D-Cu-Flo.@AuNPs-Cys	Electrochemiluminescence /Colorimetric	1.0×10^{-6}-5.0×10^{-2}	1.27×10^{-7}	This paper

sensitivity for AFP (1.92×10^{-8} ng mL^{-1}) and glucose (1.27×10^{-7} mol L^{-1}). Besides, a dual-channel methods can verify each other and improve the accuracy of sensors, which meets the requirements of fast screening and quantitative analysis. The satisfactory analytical results in human serum/urine samples also demonstrated the applicability of the proposed method in physiological sample matrix. We believe that this effective and promising bimodal ECL-technology paves a new avenue for the early clinical diagnostics and biomedical research, especially in developing countries with very limited modern instruments.

Supporting information available

The lists of instruments and reagents; Processes of fabrication of 3D GCE/Cu-Flo. and the preparation of real samples; Optimization of the conditions for GCE/Cu-Flo. Preparation: Effects of the number of electrodeposition cycles for GO (Fig. S1). Effects of electrodeposition and oxidation time on the current-response of the sensor (Fig. S2). SEM image of GCE/Cu-Flo.@AuNPs (Fig. S3). The AFM 3D-image of Cu-Flo. NMs (Fig. S4). XRD spectra of Cu-based nanosheet micro-flowers GCE/Flo (Fig. S5). Effect of pH value of the solution with 0.2 mol L^{-1} PBS containing 50 mmol L^{-1} glucose; Effect of the concentration of luminol on ECL intensity in 0.2 mol L^{-1} PBS (pH = 9.0) containing 50 mmol L^{-1} glucose; Different concentrations of Biotin-AFP antibody caused ECL-changes of GCE/Cu-Flo.@AuNPs-Cys-luminol; Incubation time of the AFP on GCE/Cu-Flo.@AuNPs-Cys-luminol/$Anti_{AFP}$ (Fig. S6A-D). Effect of the temperature of GCE/Cu-Flo.@AuNPs-Cys-luminol on ECL intensity in 0.2 mol L^{-1} PBS (pH = 9.0) containing 50 mmol L^{-1} glucose (Fig. S7). The durability of Cu-Flo.@AuNPs-Cys on ECL intensity in 0.2 mol L^{-1} PBS (pH = 9.0) containing 50 mmol L^{-1} glucose (Fig. S8). The reproducibility of Cu-Flo.@AuNPs-Cys on ECL intensity in 0.2 mol L^{-1} PBS (pH = 9.0) containing 50 mmol L^{-1} glucose (Fig. S9). Interference tests of the fabricated sensor for glucose catalysis (Fig. S10). The actual photo of the developed ECL sensor with ECL emission (A); picture of the working electrodes (a-b) and top view of the working electrode with magnified Cu-Flo. NMS nanomaterial Fig. S11 (B). The electrically active areas of bare GCE, GCE/rGO, GCE/CuNPs and GCE/Cu-Flo.@AuNPs (Table S1). Comparison of different methods for the determination of AFP (Table S2). Results for assay of glucose in human serum samples (n = 3) (Table S3). The determination of glucose in human urine from healthy individuals (n = 3) (Table S4). Recovery experiments for sensing AFP in the spiked serum samples from human (Table S5). Comparison of colorimetric measurement and ECL measurement using the dual-modal ECL-biosensor for the determination of glucose (Table S6).

CRediT authorship contribution statement

Jianping Guo: Visualization, Investigation, Data curation, Writing – original draft, Writing – review & editing. **Shijie Li:** Data curation, Writing – review & editing. **Junying Wang:** Conceptualization, Methodology, Writing – review & editing. **Junping Wang:** Conceptualization, Methodology, Writing – review & editing, Supervision.

Declaration of competing interest

The authors declare that they have no known competing financial interests or personal relationships that could have appeared to influence the work reported in this paper.

Acknowledgements

This work was supported by “National Natural Science Foundation of China”(Grant No.32102068), Innovation Project of Excellent Doctorial Dissertation of Tianjin University of Science and Technology(No. 2020010) and the 68th China Postdoctoral Science Foundation (2020M680870)

Appendix A. Supplementary data

Supplementary data to this article can be found online at https://doi.org/10.1016/j.bios.2021.113820.

References

Archana, V., Xia, Y., Fang, R., Gnana kumar, G., 2019. ACS Sustainable Chemistry & Engineering, 7, pp. 6707–6719.
Bao, Y., Han, K., Ding, Z., Li, Y., Li, T., Guan, M., Li, G., 2021. Spectrochimica Acta. Part A, Molecular and Biomolecular Spectroscopy, 253, p. 119562.
Biniuri, Y., Albada, B., Wolff, M., Golub, E., Gelman, D., Willner, I., 2018. ACS Catal. 8 (3), 1802–1809.
Bowmaker, G.A., Hartl, H., Urban, V., 2000. Inorg. Chem. 39 (20), 4548–4554.
Carro, J., Ferreira, P., Martinez, A.T., Gadda, G., 2018. Biochemistry 57 (11), 1790–1797.
Chen, H., Yuan, C., Yang, X., Cheng, X., Elzatahry, A.A., Alghamdi, A., Su, J., He, X., Deng, Y., 2020. ACS App. Nano Mater. 3 (5), 4586–4598.
Chen, Z., Villani, E., Inagi, S., 2021. Curr. Opi. in Electrochem. 28, 100702.
Cheng, S., Liu, H., Zhang, H., Chu, G., Guo, Y., Sun, X., 2020. Sensor. Actuator. B Chem. 304, 127367.
Clancy, A.J., Bayazit, M.K., Hodge, S.A., Skipper, N.T., Howard, C.A., Shaffer, M.S.P., 2018. Chem. Rev. 118 (16), 7363–7408.
Ding, W., Liu, H., Zhao, W., Wang, J., Zhang, L., Yao, Y., Yao, C., Song, C., 2020. ACS App. Bio Mater. 3 (9), 5905–5912.
Du, P., Niu, Q., Chen, J., Chen, Y., Zhao, J., Lu, X., 2020. Anal. Chem. 92 (11), 7980–7986.
Duan, Y., Huang, Y., Chen, S., Zuo, W., Shi, B., 2019. ACS Omega 4 (6), 9911–9917.
Fan, Y., Cui, M., Liu, Y., Jin, M., Zhao, H., 2020. Spectrochim. Acta Mol. Biomol. Spectrosc. 228, 117735.
Geng, D., Bo, X., Guo, L., 2017. Sensor. Actuator. B Chem. 244, 131–141.
Gobel, D., Clamor, N., Lork, E., Nachtsheim, B.J., 2019. Org. Lett. 21 (14), 5373–5377.
Hu, Q., Yang, J., Zheng, Z., Ding, Y., Chen, Y., Gao, W., 2019. Biosens. Bioelectron. 143, 111627.
Huang, B.-R., Kathiravan, D., Wu, C.-W., Yang, W.-L., 2020. ACS App. Bio Mater. 3 (9), 5966–5973.
Jiang, S., Chen, Q., Lin, J., Liao, G., Shi, T., Qian, L., 2021. Sensor. Actuator. B Chem. 345, 130364.
Jiang, S., Zhang, Y., Yang, Y., Huang, Y., Ma, G., Luo, Y., Huang, P., Lin, J., 2019. ACS Appl. Mater. Interfaces 11 (11), 10554–10558.
Jie, G., Ge, J., Gao, X., Li, C., 2018. Biosens. Bioelectron. 118, 115–121.
Kang, T.L., Bei, Hao, Qinglan, Gao, Weijie, Bin, Feng, Hui, Kwun Nam, Dou, Baojuan, Fu, Dong, 2020. ACS Sustainable Chemistry & Engineering, 0c05449.
Khoshfetrat, S.M., Khoshsafar, H., Afkhami, A., Mehrgardi, M.A., Bagheri, H., 2019. Anal. Chem. 91 (9), 6383–6390.
Lee, P.-Y., Lin, L.-Y., 2021. J. Power Sources 494, 229754.
Li, D., Zhang, S., Feng, X., Yang, H., Nie, F., Zhang, W., 2019a. Sensor. Actuator. B Chem. 296, 126631.
Li, X., Sun, X., Fan, D., Yan, T., Feng, R., Wang, H., Wu, D., Wei, Q., 2019b. Biosens. Bioelectron. 142, 111551.
Liu, Z., Wang, L., Liu, P., Zhao, K., Ye, S., Liang, G., 2021. Food Chemistry, 357, p. 129753.
Luo, W.Z., Changfeng, Su, Shao, Li, Di, He, Yao, Huang, Qing, Fan, Chunhai, 2010. ACS Nano 4 (12), 7451–7458.
Ma, J., Li, Y., Liu, J., Zhao, Z., Xu, C., Wei, Y., Song, W., Sun, Y., Zhang, X., 2019. Ind. Eng. Chem. Res. 58 (6), 2389–2395.
Olvera, D., Monaghan, M.G., 2021. Advanced Drug Delivery Reviews, 170, pp. 396–424.
Praoboon, N., Siriket, S., Taokaenchan, N., Kuimalee, S., Phaisansuthichol, S., Pookmanee, P., Satienperakul, S., 2021. Food Chemistry, 366, p. 130590.
Quintero-Jaime, A.F., Quílez-Bermejo, J., Cazorla-Amorós, D., Morallón, E., 2021. Electrochim. Acta 367, 137434.
Roushani, M., Sarabaegi, M., Hosseini, H., 2021. Compos. Commun. 25, 100686.
Shen, K., Chen, X., Chen, J., Li, Y., 2016. ACS Catal. 6 (9), 5887–5903.
Singh, B., Dempsey, E., Laffir, F., 2014. Sensor. Actuator. B Chem. 205, 401–410.
Tan, K.H., Lee, H.W., Chen, J.-W., Dee, C.F., Majlis, B.Y., Soh, A.K., Wu, C.-L., Chai, S.-P., Chang, W.S., 2017. J. Phys. Chem. C 121 (25), 13487–13495.
Vinoth, V., Subramaniyam, G., Anandan, S., Valdés, H., Manidurai, P., 2021. Mater. Sci. Eng., B 265, 115036.
Wang, F., Chen, X., Chen, L., Yang, J., Wang, Q., 2019. Materials Science & Engineering. C, Materials for Biological Applications 96, pp. 41–50.
Wang, F., Liu, X., Lu, C.-H., Willner, I., 2013. ACS Nano 7 (8), 7278–7286.
Wang, J., Yang, B., Zhong, J., Yan, B., Zhang, K., Zhai, C., Shiraishi, Y., Du, Y., Yang, P., 2017. J. Colloid Interface Sci. 497, 172–180.
Wang, N., Zhao, X., Chen, H., Bai, L., Xu, H., Wang, W., Yang, H., Wei, D., Yang, L., 2020a. Reactive and Functional Polymers, 154, p. 104632.
Wang, S., Wang, M., Li, C., Li, H., Ge, C., Zhang, X., Jin, Y., 2020b. Sensor. Actuator. B Chem. 311, 127919.
Wang, X., Shang, L., Zhang, W., Jia, L.P., Ma, R.N., Jia, W.L., Wang, H.S., 2019a. Biosens. Bioelectron. 141, 111436.
Xu, D., Sun, Z.H., Hua, X., Han, H.X., Ma, W., Long, Y.T., 2020. ACS Sens. 5 (7).
Xue, J., Yang, L., Wang, H., Yan, T., Fan, D., Feng, R., Du, B., Wei, Q., Ju, H., 2019. Biosens. Bioelectron. 133, 192–198.
Yagmuroglu, O., Diltemiz, S.E., 2020. Anal. Biochem. 591, 113572.

Yang, X., Zhao, Y., Sun, L., Qi, H., Gao, Q., Zhang, C., 2018. Sensor. Actuator. B Chem. 257, 60–67.
Zhou, B., Ye, Q., Li, F., Xiang, X., Shang, Y., Wang, C., Shao, Y., Xue, L., Zhang, J., Wang, J., Ding, Y., Chen, M., Wu, Q., 2022. Sensor. Actuator. B Chem. 351, 130906.
Zhu, J., Peng, X., Nie, W., Wang, Y., Gao, J., Wen, W., Selvaraj, J.N., Zhang, X., Wang, S., 2019a. Biosens. Bioelectron. 141, 111450.
Zhu, N., Gu, L., Wang, J., Li, X., Liang, G., Zhou, J., Zhang, Z., 2019b. J. Phys. Chem. C 123 (14), 9388–9393.
Zhu, X., Liu, H., Dai, Y., Wang, X., Luo, C., Wei, Q., 2020. Biosens. Bioelectron. 151, 111970.
Zhu, Y., Zhang, Q., Li, X., Pan, H., Wang, J., Zhao, Z., 2019c. Sensor. Actuator. B Chem. 293, 53–58.
Zhuang, X., Han, C., Zhang, J., Sang, Z., Meng, W., 2021. J. Electroanal. Chem. 882, 115040.
Zou, C., Yang, B., Bin, D., Wang, J., Li, S., Yang, P., Wang, C., Shiraishi, Y., Du, Y., 2017. J. Colloid Interface Sci. 488, 135–141.